Optical design of the NASA-NSF extreme precision Doppler spectrograph concept "WISDOM"

Stuart I. Barnes[a], Gábor Fűrész[b], Robert A. Simcoe[b], Stephen A. Shectman[c], and Deborah F. Woods[d]

[a] Stuart Barnes Optical Design (Germany);
[b] MIT Kavli Institute for Astrophysics and Space Research (United States);
[c] Carnegie Observatories (United States);
[d] MIT Lincoln Lab. (United States).

ABSTRACT

The WISDOM instrument concept was developed at MIT as part of a NASA-NSF funded study to equip the 3.5 m WIYN telescope with an extremely precise radial velocity spectrometer. The spectrograph employs an asymmetric white pupil optical design, where the instrument is split into two nearly identical "Short" (380 to 750 nm) and "Long" (750 to 1300 nm) wavelength channels. The echelle grating and beam sizes are $R3.75/125$ mm and $R6/80$ mm in the short and long channels respectively. Together with the pupil slicer, and octagonal to rectangular fibre coupling, this permits resolving powers over $R = 120$k with a $1.2''$ diameter fibre on the sky. A factor of two reduction in the focal length between the main collimator OAP and the transfer collimator ensures a very compact instrument, with a small white pupil footprint, thereby enabling small cross-dispersing and camera elements. A dichroic is used near the white pupil to split each of the long and short channels into two, so that the final spectrograph has 4 channels; namely "Blue", "Green", "Red" and "NIR". Each of these channels has an anamorphic VPH grism for cross-dispersion, and a fully dioptric all-spherical camera objective. The spectral footprints cover 4k×4k and 6k×6k CCDs with 15 μm pixels in the short "Blue" and "Green" wavelength channels, respectively. A 4k×4k CCD with 15 μm pixels is used in the long "Red" channel, with a HgCdTe 1.7 μm cutoff 4k×4k detector with 10um pixels is to be used in the long "NIR" channel. The white pupil relay includes a Mangin mirror very close to the intermediate focus to correct the white pupil relay Petzval curvature before it is swept into a cylinder by the cross-dispersers. This design decision allows each of the dioptric cameras to be fully optimised and tested independently of the rest of the spectrograph. The baseline design for the cameras also ensures that the highest possible (diffraction limited) image quality is achieved across all wavelengths, while also ensuring insensitivity of spot centroid locations to variations in the pupil illumination. This insensitivity is proven to remain even in the presence of reasonable manufacturing and alignment tolerances. Fully ray-traced simulations of the spectral formats are used to demonstrate the optical performance, as well as to provide pre-first-light data that can be used to optimise the data reduction pipeline.

Keywords: Extreme precision radial velocity spectrograph, asymmetric white pupil échelle spectrograph, anamorphic VPH grisms.

1. INTRODUCTION

The WISDOM instrument concept was developed as part of a NASA-NSF funded study to equip the 3.5 m WIYN telescope with an extremely precise radial velocity spectrometer. A general overview of the instrument is presented elsewhere in these proceedings by Fűrész et. al.[1] WISDOM is fed from the telescope using a combination of octagonal and rectangular core fibres, together with an optical double scrambler. The fibre feed includes an ADC and tip-tilt mirror for maximising throughput, as well as a novel pupil slicer. Detailed descriptions of these aspects of the instrument are also presented elsewhere in these proceedings by Fűrész et. al.[2] This paper will concentrate on the spectrograph optical design.

Ground-based and Airborne Instrumentation for Astronomy VI, edited by Christopher J. Evans, Luc Simard, Hideki Takami
Proc. of SPIE Vol. 9908, 99086J · © 2016 SPIE · CCC code: 0277-786X/16/$18 · doi: 10.1117/12.2232352

2. OVERVIEW

The WISDOM spectrograph is split into a "Short" wavelength channel ($\lambda\lambda$ = 380 to 750 nm) and a "Long" wavelength channel ($\lambda\lambda$ = 750 to 1300 nm). Both the short wavelength channel (SWC) and long wavelength channel (LWC) spectrographs follow very similar asymmetric white pupil optical designs*. That is, they both have primary off-axis parabolic collimators with a focal length $f_1 = 1000$ mm, however the collimated beam sizes are 125 mm and 80 mm in the SWC and LWC channels respectively. The slightly ellipsoidal ($k \approx -0.91$) secondary (or transfer) collimator has a focal length of $f_2 = 500$ mm. The asymmetry factor ($f_1/f_2 = 2$) is used to reduce the overall size of the instrument, while also allowing significantly smaller cross-dispersers and camera lenses than would be possible with symmetric designs. An asymmetric design can also be used more efficiently with VPH cross-dispersing elements. The SWC and LWC spectrographs have echelle gratings with different blaze angles (θ_B) and line densities (T). That is, in the SWC $\theta_B = 75.1°$ ($R3.75$) and $T = 31.6$ lines/mm while the LWC grating has $\theta_B = 80.7°$ ($R6.11$), and $T = 13.33$ lines/mm. Together with the pupil slicer, and octagonal to rectangular fibre coupling, this permits resolving powers ($R = \lambda/\Delta\lambda$) over $R = 120,000$ with a 1.2″ fibre on the sky.

Near the location of the white pupil, a dichroic is used to again divide each of the short and long wavelength channels†. This maximizes the (average) spatial order separation, while minimizing the (combined) detector real estate required for complete wavelength coverage. This splitting also makes it possible to fully optimize the efficiency of the VPH cross-disperser given the relatively narrow band-pass, and it also allows the highest performance antireflection (and reflective) coatings to be applied to all single-channel optics. The final geometry of the WISDOM spectrograph is the result of an optimization of the wavelength distributions across the four available channels, given a limited number of detector choices, with the constraint that each resolution element must be sampled by at least 3.5 pixels, and that there also be sufficient (minimum) inter-order separation in all four channels for the multiple-fibre entrance slit. Some additional effort is made to arrange the reflection angle of the dichroic, together with the VPH grism parameters, so that the optical axes of the three shorter wavelength cameras are parallel to the optical axes of the two collimators. This was done in order to simplify the mechanical assembly, via an easily identified reference axis (that will also be used optically for additional alignment tasks), and also to minimize the overall instrument volume. This adjustment was not performed on the NIR camera in order to allow the detector to be raised somewhat closer to the top of the vacuum tank. Further details of the intermediate focus Mangin mirror, the VPH grisms, and the four camera objectives will be given below. Fig. 1 shows the layout of the SWC spectrograph. A summary of the spectrograph parameters can be found in Table 1. Image quality details are also given below.

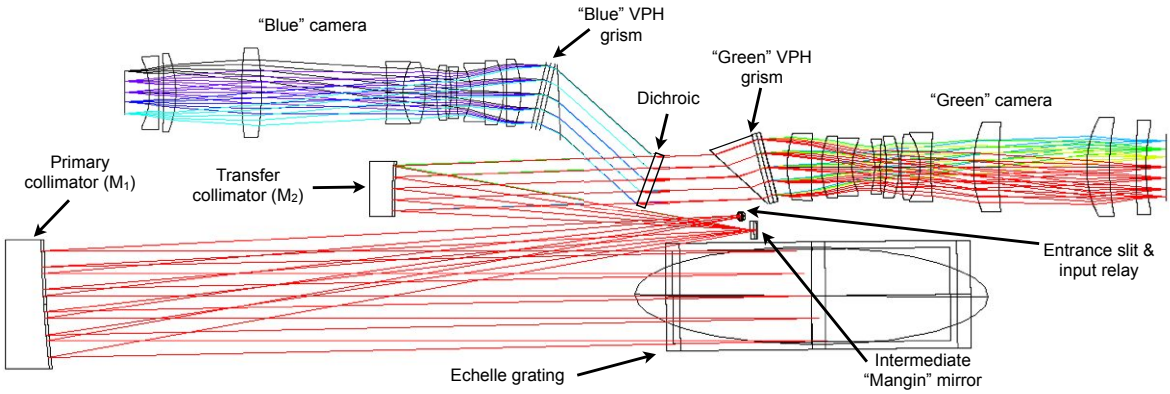

Figure 1. The optical layout of the WISDOM short wavelength channel (SWC) spectrograph. The (z-)distance from the primary mirror vertex to the detector optical plane is 1575 mm. The échelle dispersion direction is normal to the page. Note that the LWC spectrograph is very similar in form and is placed immediately adjacent to the SWC, but with a flipped échelle dispersion direction. See Fűrész et. al[1] elsewhere in this proceedings for further details.

*Existing examples of this design form include SALT HRS (Barnes et al., 2008[3]) and KiwiSpec (Gibson et al., 2012[4]).

†Multi-channel designs of this type have been discussed in Barnes et al., 2008[5] (i.e., the "Q-Spec" concept for the GMT HROS) and Barnes et al., 2012[6] (i.e., the "KiwiSpec-GHOST" concept for Gemini).

Table 1. Summary of the WISDOM spectrograph optical properties.

	Short wavelength channel (SWC)		Long wavelength channel (LWC)	
Channel:	"Blue"	"Green"	"Red"	"IR"
Wavelength range:	378.7–495.2 nm	483.4–769.2 nm	749.7–952.2 nm	934.2–1316.1 nm
Order numbers:	161–124, ($n = 38$)	126–80, ($n = 47$)	197–156, ($n = 42$)	158–113, ($n = 46$)
Resolving power:	$R = 120$k ($n = 3.54$ pixels)		$R = 120$k ($n = 3.50$ pixels)	
Beam size:	$B = 125$ mm		$B = 80$ mm	
Primary collimator:	$f_1 = 1000$ mm ($f/8$ OAP, $\theta = 6.5°$)		$f_1 = 1000$ mm ($f/12.5$ OAP, $\theta = 6.5°$)	
Echelle:				
Blaze angle:	$\theta_B = 75.1°$ ($R3.75$)		$\theta_B = 80.7°$ ($R6.11$)	
Line density:	$T = 31.6$ mm^{-1}		$T = 13.33$ mm^{-1}	
Ruled area:	130×400 mm		100×400 mm	
Mangin mirror:				
Glass, size:	S-FSL5, 25×120 mm		S-FSL5, 25×145 mm	
Thic., off-axis dist.:	$t = 8.7$ mm, $\Delta y \approx 21.5$ mm		$t = 8.7$ mm, $\Delta y \approx 21.5$ mm	
Secondary collimator:	$f_2 = 500$ mm, $k \approx -0.91$		$f_2 = 500$ mm, $k \approx -0.91$	
Cross-dispersing grisms:				
VPH line density:	1125 mm^{-1}	620 mm^{-1}	945 mm^{-1}	565 mm^{-1}
VPH AOI (cwl):	9.45°	7.35°	15.62°	12.19°
Prism glass:	S-BSL7	S-BSL7	S-BSL7	S-BSL7
Prism AOI	$\theta_i = 45.0°$	$\theta_i = 45.0°$	$\theta_i = 45.0°$	$\theta_i = 50.0°$
Prism apex angle:	$\alpha = 27.6°$	$\alpha = 27.8°$	$\alpha = 27.9°$	$\alpha = 30.6°$
Anamorphic factor:	$B_{out}/B_{in} = 1.25$	$B_{out}/B_{in} = 1.25$	$B_{out}/B_{in} = 1.08$	$B_{out}/B_{in} = 1.31$
Cameras:				
Focal length:	$f_{cam} = 425.1$ mm	$f_{cam} = 425.1$ mm	$f_{cam} = 258.2$ mm	$f_{cam} = 172.1$ mm
Focal ratio (X):	$f/D_x = 6.8$	$f/D_x = 6.8$	$f/D_x = 6.5$	$f/D_x = 4.3$
Focal ratio (Y):	$f/D_y = 5.5$	$f/D_y = 5.5$	$f/D_y = 6.0$	$f/D_y = 3.3$
Detector:				
Type:	CCD	CCD	CCD	H4RG
Format (approx.):	4096×4096	6144×6144	4096×4096	4096×4096
Pixel size:	15 μm	15 μm	15 μm	10 μm

3. INTERMEDIATE FOCUS "MANGIN" MIRROR TRADE STUDY

The white pupil relay includes correcting lens with a reflecting internal surface very close to the intermediate focus. The use of a "Mangin" mirror element is also described in detail by Furesz et al. 2014.[7] Its purpose is to correct the white pupil relay Petzval curvature present at the intermediate focus *before* it is swept into a cylinder by the cross-dispersers. This eliminates the requirement to include a cylindrical lens very close to the detector in order to correct this curvature. Invariably, as is common in most other spectrographs of this form, a cylindrical (or otherwise non-rotationally symmetric) lens cannot provide complete correction, and its placement very close to the detector surface complicates the design and alignment of the detector assembly. The use of an intermediate focus Mangin mirror allows each of the dioptric cameras to be fully optimised and tested *independently of the rest of the spectrograph* without placing any constraints on the actual form of the camera lenses.

The Mangin mirror to be used in WISDOM is formed from an off-axis section of a concave/convex singlet lens. This has proven to be possible after a trade-study between (i) spherical and (ii) toroidal designs, in addition to a comparison with (iii) designs without a Mangin mirror element (see Figure 2). For each of the studies (i) & (ii), a spectrograph model was created with a paraxial camera lens and a flat detector plane. However, study (iii) used a paraxial camera together with a cylindrical detector plane. The latter model represents the "classical" form of white pupil spectrograph, such as has been implemented in FEROS,[8] UVES,[9] HRS[10],[11] HARPS[12] etc, but with a "perfect" field-flattening lens. While the toroidal Mangin lens design gave the best image quality for a single (central) field location, a spherical design ensured the best average image quality over the extent of the WISDOM entrance slit. The uncorrected "classical" design has the worst overall image quality, even though the model assumes perfect correction of the Petzval curvature by using a cylindrical detector.

It should also be emphasised that this result remains valid *independently of the form of the spectrograph camera optics*, and therefore the result can be transferred to any scaling of this form of instrument. Furthermore, to clarify, it is possible to ensure that all ghosts (both front surface reflections, and internal double-reflections) can be fully mitigated by slightly adjusting the "y-axis" offset of the parent lens. This effectively introduces a small wedge in the lens, thereby allowing the ghosts to be redirected away from any other element, and image quality is not affected. A high quality anti-reflection coating can be applied to the transmissive surface of the Mangin mirror in order to further mitigate against stray light.

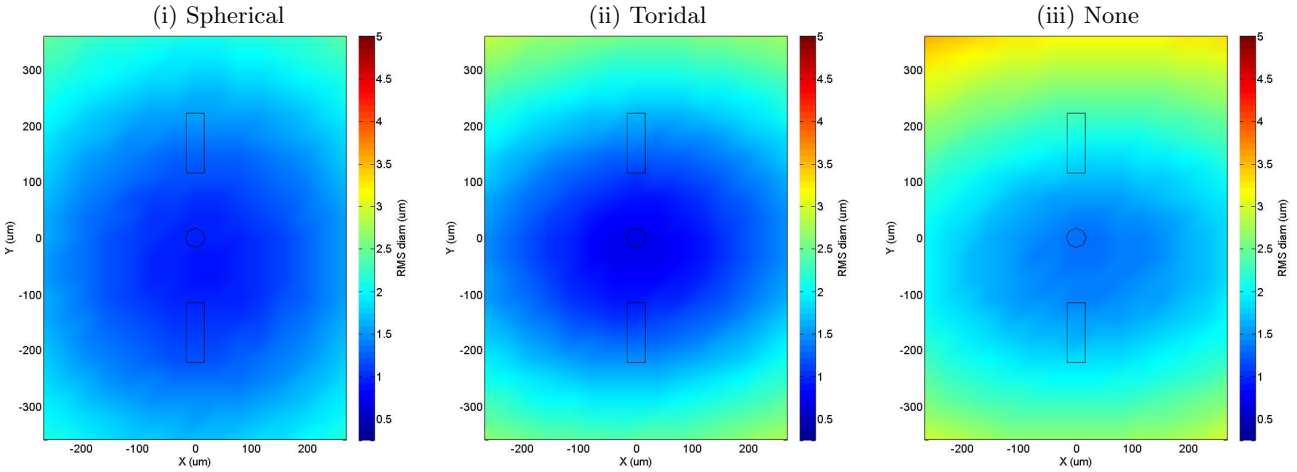

Figure 2. Results from the Mangin mirror trade-study for a (i) spherical lens, (ii) a toroidal lens, and (iii) no lens but assuming a cylindrical detector. In each case, the image quality averaged over all wavelengths (within the free spectral range) is shown as a function of the point of origin at the entrance slit. The format of the nominal entrance slit to be used for WISDOM is shown (black lines). A Mangin mirror formed from a section of a fully spherical lens clearly produces the best and most uniform image quality across an extended entrance slit.

4. ANAMORPHIC VPH GRISMS

The multi-channel design of WISDOM is ideal for the use of volume phase holographic (VPH) gratings cross-dispersers. Based on experience with similar instruments, the peak efficiency of VPH grating cross-dispersers can exceed 85 to 90% for the specified wavelength ranges and line densities. Given the conservative bandwidths of each channel, the minimum cross-disperser efficiency should also exceed 70 to 75%. In addition, the efficiency envelope of the VPH gratings can in principle be tuned to mitigate other aspects of the design.

Each of the four VPH gratings are designed to be used together with an S-BSL7 prism on the entrance face. This provides a spatial anamorphic factor ranging from $B_{\rm out}/B_{\rm in} = 1.25$ in the Blue/Green channels, to $B_{\rm out}/B_{\rm in} = 1.08$ and 1.31 in the Red and NIR channels respectively The anamorphism allows a spatial compression of slit image, which increases the effective inter-order separation, while also slightly reducing the number of pixels required to read out the slit image. As noted above, the orientation and dispersive properties of these gratings can be tuned in order to position the camera optical axes. Finally, it is also important to introduce a slight Littrow angle at the grating surface in order to avoid VPH recombination ghosts (Burgh et al., 2007[13]).

5. CAMERAS AND DETECTORS

The focal lengths, and fields of view of each of the cameras have been adjusted so that a minimum of 3.5 pixels sample each $R \approx 120\,000$ resolution element. The baseline design for the camera lenses ensures that the highest possible (near diffraction limited) image quality is achieved across all wavelengths, while also ensuring insensitivity of spot centroids to any variation in the pupil illumination. The preliminary camera design (see Fig. 3) has 9 all spherical lenses in 7 groups in addition to a fused silica detector entrance window. Aspheric and off-axis and/or decentred elements have been completely avoided so as to limit the additional risks and costs associated

with these items. It is emphasised that the number of camera optical elements has a *negligible effect on the overall instrument throughput* owing the fact that all surfaces will have excellent anti-reflection coatings thanks to the narrow band-pass of each channel in the 4-channel design. An effort has been made to make all four cameras as nearly similar to one another as possible, however given the large variation in focal length and field of view, the final camera designs differ slightly. It has also been possible to ensure a high degree of telecentricity, as a potential mitigation against any possible defocus induced image drift. This requirement, together with the fact that the entrance pupil is actually smaller than the size of the dectector, results in a somewhat unusual camera layout. Nevertheless, the preliminary design form has proven to be extremely compact; i.e., the length of the green camera is ∼530 mm for a 425 mm focal length. In order to further mitigate against the potential for far-field illumination variations to also cause centroid drifts, the optical prescriptions of each camera are further tuned in order to minimize this possibility (see Sec. 7 for further details). The image quality of the green channel camera is shown in Fig. 4 and 5.

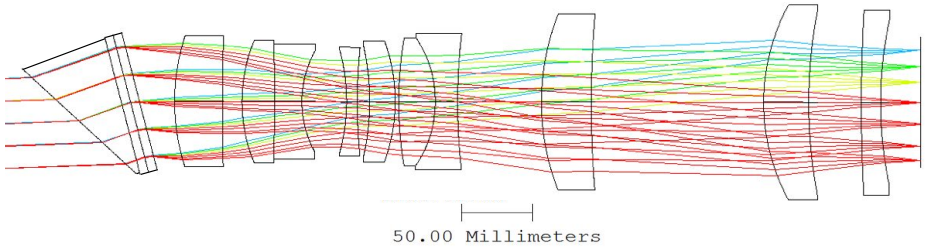

Figure 3. The preliminary camera objective for the WISDOM "Green" channel. This camera has a focal length of 425 mm and is 530 mm in length. The anamorphic VPH grism cross-disperser is also shown on the left. The image quality of WISDOM with this camera is shown in Fig. 4 and 5. In addition to being near-diffraction limited, the camera focal plane is highly telecentric. The camera has also been optimised to ensure immunity to any pupil illumination variations.

Figure 4. Image quality of the preliminary WISDOM green channel camera. The spot diagrams uniformly cover the spectral format in this channel (see Fig. 6). Each box is one pixel square. The RMS diameter ($\phi_{\rm rms}$) is shown above each pixel. Note that each pixel maintains 100% ensquared energy. See Fig. 5 for the corresponding PSF images.

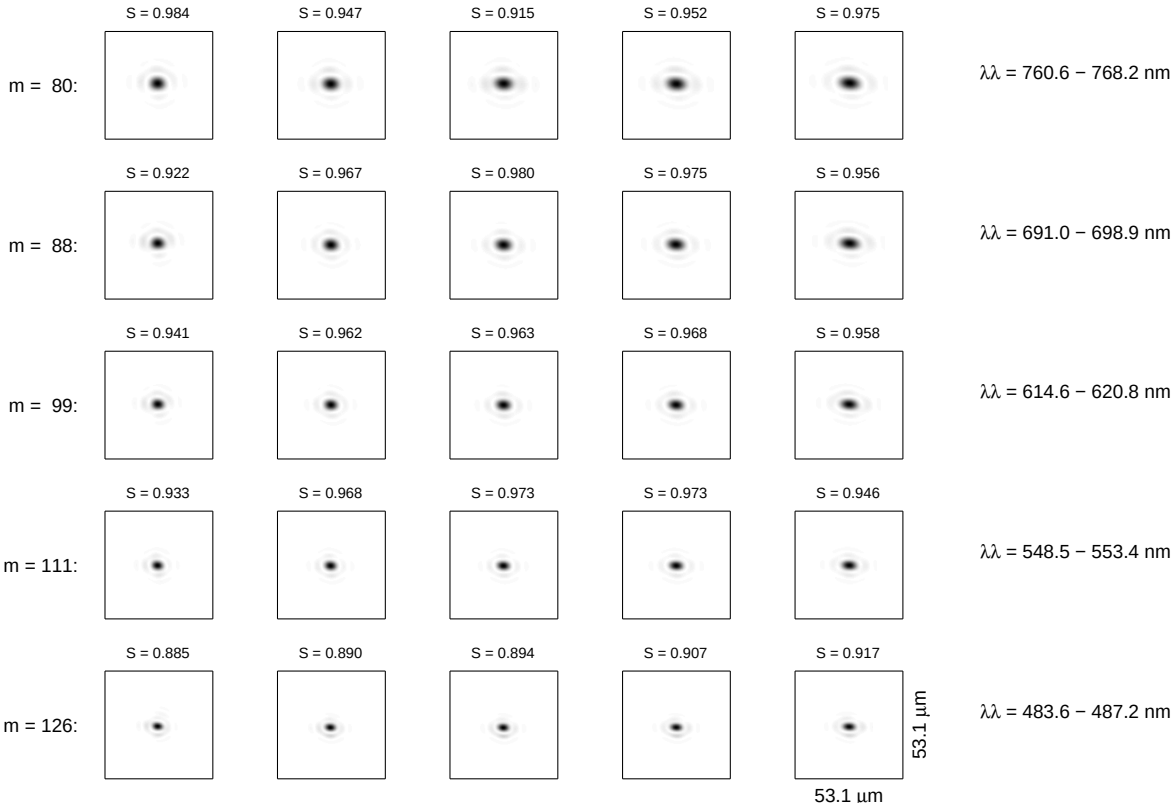

Figure 5. Image quality of the preliminary WISDOM green channel camera. The point source PSF images uniformly cover the spectral format in this channel (see Fig. 6). Each box is one resolution element (3.5 pixels) square. The Strehl ratio (S) is shown above each box. See Fig. 4 for the corresponding spot diagrams.

The spectral footprints cover 4k×4k and 6k×6k CCDs with 15 μm pixels in the "Blue" and "Green" wavelength channels respectively. A 4k×4k CCD with 15 μm pixels is used in the "Red" channel, with a HgCdTe 1.7 μm cutoff 4k×4k detector with 10 μm pixels is to be used in the "NIR" channel. See Fig. 6 for the green channel format together with a map of RMS image quality. The formats for the other channels are similar (for their respective wavelength ranges) and have identical image quality properties (scaled to the nominal pixel size).

6. SYNTHETIC IMAGES

Synthetic spectral images for each of the WISDOM channels have been created using ray-tracing methods with the EchMod package (Barnes 2012[14]). This makes it possible to create fully realistic spectra *during* the initial instrument design phase and *ahead* of final construction (see Fig. 7 for an example). The intention of this process is to fully validate the data reduction pipeline well in advance of instrument commissioning. In addition, these methods also allow the verification of instrumental stability, given the possibility of updating and adjusting the instrument optical model according to mechanical, environmental, and illumination perturbations. The issue of pupil illumination variability is further discussed in Sec. 7 below.

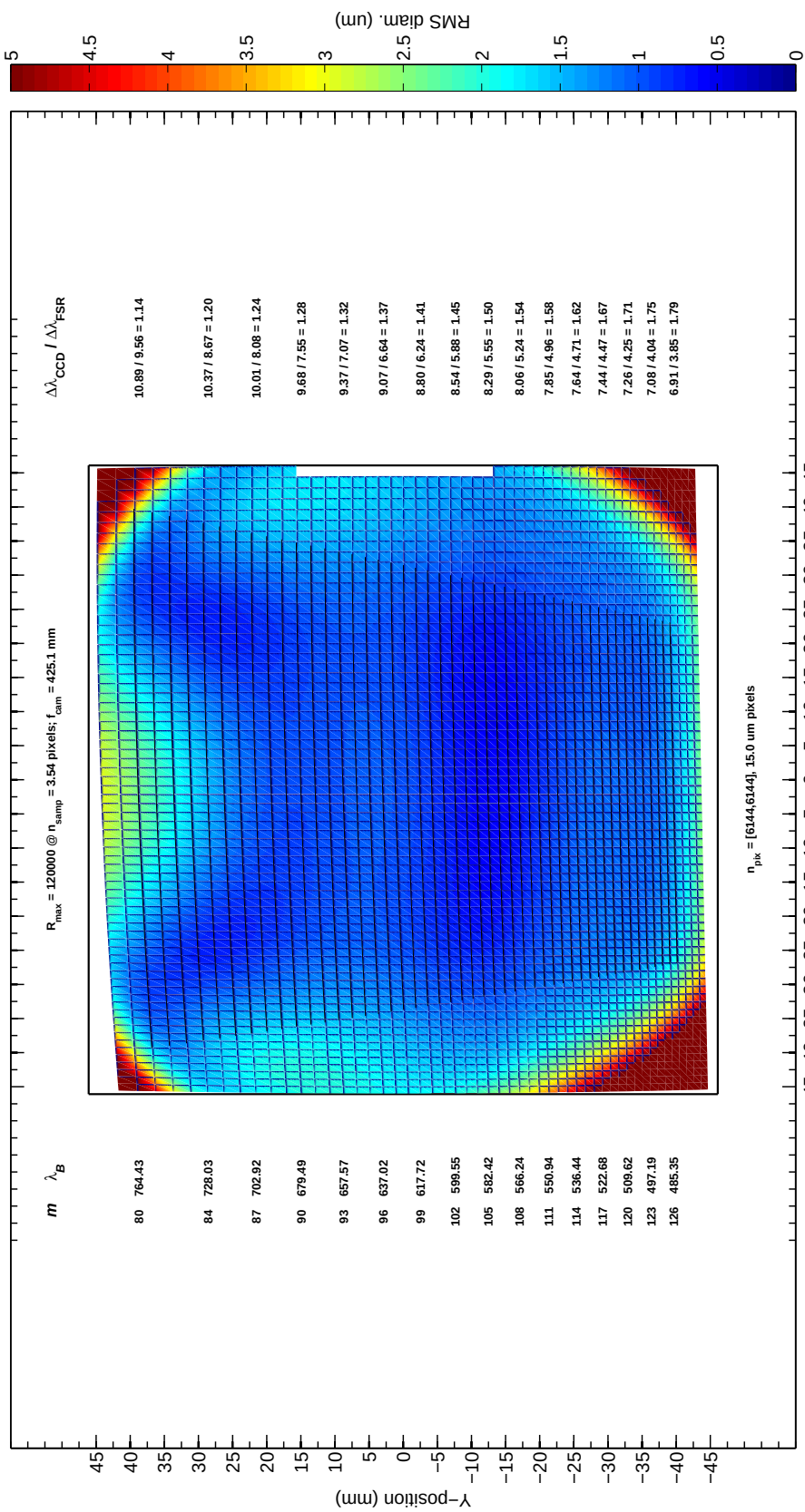

Figure 6. The WISDOM spectrograph "Green" channel spectral format. The order numbers (m) and blaze wavelengths (λ_B) are shown on the left, while the ratio between the wavelength extent of a single free spectral range ($\Delta\lambda_{FSR}$) and the full coverage of the detector ($\Delta\lambda_{CCD}$) is shown on the right. The colormap indicates the RMS spot diameter as a function of location on the detector. Note that the image quality is uniformly excellent everywhere within the free spectral range (solid lines). The spectral formats and image quality maps are similar in the "Blue", "Red" and "NIR" channels.

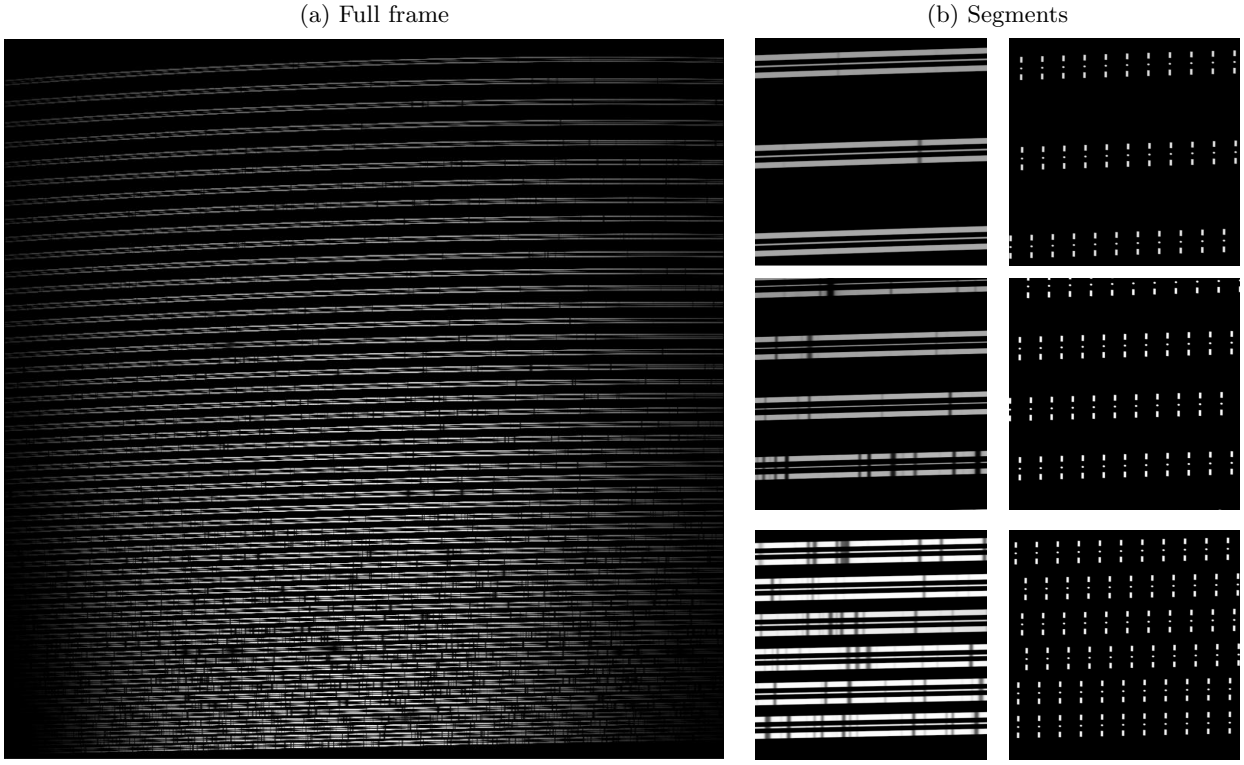

Figure 7. Synthetic spectra for the WISDOM "Green" channel. Left (a) shows a full frame spectrum with a solar-like input. Right (b) shows segments of full frame spectra (solar-like and calibration) taken from the top, middle, and bottom of the frame. This makes it possible to see the generous inter-slice and inter-order separations.

7. PUPIL ILLUMINATION STABILITY STUDY

While every effort is taken in order to design the mechanical and environmental mountings and enclosures so as to ensure the absolute stability of the WISDOM spectrograph, in addition to excellent wavelength calibration accuracy, the radial velocity precision also relies on having very stable illumination of the spectrograph optics. For the WIYN telescope instrument, this issue is addressed by the design of the pupil slicer and scrambling fibre optic train, details of which can be found elsewhere in these proceedings.[2] Nevertheless, the possibility still remains that some residual illumination variability will remain, and that this will impart a systematic offset in any one radial velocity observation. In order to examine and address this concern, a detailed study of the spectrographs performance was made in the presence of a range of pupil illumination variations.

The method follows that of various pervious similar studies (e.g., Fúrész et. al, 2014[7] and Stürmer et al, 2014[15]). That is, first, a set of ray-traces was performed where the inner 50% and the outer 50% of the entrance pupil was illuminated. These ray-traces use a grid of some 51 wavelength spaced uniformly across all orders. Next, for each simulated "observation" a linear combination of these two inner and outer ray traces was made, and the location of the resulting spot was compared to that of a spot created from a fully (uniformly) illuminated ray-trace. The assumption behind this approach is that the combination of octagonal and rectangular fibres which are used in WISDOM together with a fibre double-scrambler (see op. cit. above), will ensure complete azimuthal scrambling. However, it remains possible that slight radial illumination variations will remain, and furthermore, that these variations will not necessarily be stable in time (e.g., Avila et. al, 2012[16]).

As previous work has demonstrated (see op. cit. above), it is possible to design the spectrograph optics in order to mitigate these remaining pupil variations. In the WISDOM spectrograph, these concerns are largely eliminated simply by ensuring the highest possible image quality. However, during the final iteration of the camera optics, a pupil illumination stability factor was included in the merit function, and by this means the

ideal optical design could be rendered absolutely impervious to any radial pupil illumination variability. However, this *does not necessarily imply that the as-built spectrograph will also be impervious* as this immunity can only be realised if the spectrograph optics are built and aligned *exactly* as specified. For the purposes of illustrating this effect, from a pool of 100 randomly generated models with standard manufacturing and alignment tolerances[‡], a set of 10 spectrograph models were selected for detailed analysis. It was found that a ±1% illumination variation results in an RMS velocity shift of 46 cms^{-1}, with a linearly increasing effect as a function of increasing pupil illumination fraction. With somewhat tighter tolerances, a ±1% illumination variation was found to result in an RMS velocity shift of 30 cms^{-1}. The implication is that when the spectrograph has been fully assembled, there is a statistically significant chance that the as-built performance will be sensitive to pupil illumination variations at the RMS values. Nevertheless, there is also a non-zero probability that the performance will be equal to the ideal design simply as a matter of chance; that is, that the illumination sensitivity contribution of individual elements adds to zero. However, it is concluded that that the inclusion of manufacturing and alignment tolerances is critical to the spectrographs precision radial velocity performance. Furthermore, it is suggested that this effect will be present at some level in *all* precision radial velocity spectrographs.

8. SUMMARY

The detailed optical design of an extremely precise radial velocity spectrometer has been presented. This concept was developed as part of a NASA-NSF funded study to equip the 3.5 m WIYN telescope with an EPRV instrument. By using a dual-spectrograph 4-channel design with an asymmetric white pupil form, together with anamorphic VPH cross-dispersing grisms, and simple all-spherical dioptric cameras, an extremely compact, highly efficient, low risk concept has been demonstrated. The excellent image quality, high telecentricty, and immunity to pupil illuminations variations all contribute to improving the precision radial velocity performance. This concept study also introduces the technique of including the effects of manufacturing and alignment tolerances as part of the pupil illumination stability contribution to the radial velocity error budget.

ACKNOWLEDGMENTS

This work was funded in part through the NASA program NNH14ZDA001N-EPDS. This research has made use of NASA's Astrophysics Data System.

REFERENCES

[1] Fúrész, G., Barnes, S. I., Buchhave, L. A., Egan, M. D., Foster, R., Hellickson, T., Malonis, A., Phillips, D. F., Shectman, S. A., Simcoe, R. A., Walsworth, R. L., Winn, J., and Woods, D. F., "WISDOM: the WIYN spectrograph for doppler monitoring: a NASA-NSF concept for an extreme precision radial velocity instrument in support of TESS," in [*Ground-based and Airborne Instrumentation for Astronomy VI*], Evans, C. J. and Takami, H., eds., *Proc. SPIE* **9908** (2016).

[2] Fúrész, G., Pawluczyk, R., and Fournier, P., "Fiber link design for the NASA-NSF extreme precision doppler spectrograph concept "WISDOM"," in [*Ground-based and Airborne Instrumentation for Astronomy VI*], Evans, C. J. and Takami, H., eds., *Proc. SPIE* **9908** (2016).

[3] Barnes, S. I., Cottrell, P. L., Albrow, M. D., Frost, N., Graham, G., Kershaw, G., Ritchie, R., Jones, D., Sharples, R., Bramall, D., Schmoll, J., Luke, P., Clark, P., Tyas, L., Buckley, D. A. H., and Brink, J., "The optical design of the Southern African Large Telescope high resolution spectrograph: SALT HRS," in [*Ground-based and Airborne Instrumentation for Astronomy II*], *Proc. SPIE* **7014**, 70140K (July 2008).

[4] Gibson, S., Barnes, S. I., Hearnshaw, J., Nield, K., Cochrane, D., and Grobler, D., "KiwiSpec - an advanced spectrograph for high resolution spectroscopy: prototype design and performance," in [*Ground-based and Airborne Instrumentation for Astronomy IV*], *Proc. SPIE* **8446**, 844648 (Sept. 2012).

[5] Barnes, S. and MacQueen, P., "Q-Spec: a concept for the Giant Magellan Telescope high resolution optical spectrograph," in [*Ground-based and Airborne Instrumentation for Astronomy II*], *Proc. SPIE* **7014**, 70141H (July 2008).

[‡]The centration and tip/tilt of each lens element was found to have the highest sensitivity.

[6] Barnes, S. I., Gibson, S., Nield, K., and Cochrane, D., "KiwiSpec - an advanced spectrograph for high resolution spectroscopy: optical design and variations," in [*Ground-based and Airborne Instrumentation for Astronomy IV*], *Proc. SPIE* **8446**, 844688 (Sept. 2012).

[7] Fúrész, G., Epps, H., Barnes, S., Podgorski, W., Szentgyorgyi, A., Mueller, M., Baldwin, D., Bean, J., Bergner, H., Chun, M.-Y., Crane, J., Evans, J., Evans, I., Foster, J., Gauron, T., Guzman, D., Hertz, E., Jordán, A., Kim, K.-M., McCracken, K., Norton, T., Ordway, M., Park, C., Park, S., Plummer, D., Uomoto, A., and Yuk, I.-S., "The G-CLEF spectrograph optical design," in [*Ground-based and Airborne Instrumentation for Astronomy V*], *Proc. SPIE* **9147**, 91479G (July 2014).

[8] Kaufer, A., Wolf, B., Andersen, J., and Pasquini, L., "FEROS, the fiber-fed extended range optical spectrograph for the ESO 1.52-m telescope.," *The Messenger* **89**, 1–4 (Sept. 1997).

[9] Dekker, H., D'Odorico, S., Kaufer, A., Delabre, B., and Kotzlowski, H., "Design, construction, and performance of UVES, the echelle spectrograph for the UT2 Kueyen Telescope at the ESO Paranal Observatory," in [*Optical and IR Telescope Instrumentation and Detectors*], Iye, M. and Moorwood, A. F., eds., *Proc. SPIE* **4008**, 534–545 (Aug. 2000).

[10] Tull, R. G., "High-resolution fiber-coupled spectrograph of the Hobby-Eberly Telescope," in [*Optical Astronomical Instrumentation*], D'Odorico, S., ed., *Proc. SPIE* **3355**, 387–398 (July 1998).

[11] MacQueen, P. J., South, B. J., Strubhar, J. L., Wesley, G. L., Odoms, P. S., Edmonston, R. D., and Barnes, S. I., "The Hobby Eberly Telescope High Resolution Spectrograph upgrade," in [*Ground-based and Airborne Instrumentation for Astronomy*], Evans, C. J. and Takami, H., eds., *Proc. SPIE* **9908** (2016).

[12] Pepe, F., Mayor, M., Rupprecht, G., Avila, G., Ballester, P., Beckers, J.-L., Benz, W., Bertaux, J.-L., Bouchy, F., Buzzoni, B., Cavadore, C., Deiries, S., Dekker, H., Delabre, B., D'Odorico, S., Eckert, W., Fischer, J., Fleury, M., George, M., Gilliotte, A., Gojak, D., Guzman, J.-C., Koch, F., Kohler, D., Kotzlowski, H., Lacroix, D., Le Merrer, J., Lizon, J.-L., Lo Curto, G., Longinotti, A., Megevand, D., Pasquini, L., Petitpas, P., Pichard, M., Queloz, D., Reyes, J., Richaud, P., Sivan, J.-P., Sosnowska, D., Soto, R., Udry, S., Ureta, E., van Kesteren, A., Weber, L., Weilenmann, U., Wicenec, A., Wieland, G., Christensen-Dalsgaard, J., Dravins, D., Hatzes, A., Kürster, M., Paresce, F., and Penny, A., "HARPS: ESO's coming planet searcher. Chasing exoplanets with the La Silla 3.6-m telescope," *The Messenger* **110**, 9–14 (Dec. 2002).

[13] Burgh, E. B., Bershady, M. A., Westfall, K. B., and Nordsieck, K. H., "Recombination Ghosts in Littrow Configuration: Implications for Spectrographs Using Volume Phase Holographic Gratings," *PASP* **119**, 1069–1082 (Sept. 2007).

[14] Barnes, S. I., "EchMod: a MATLAB toolbox for modeling high resolution échelle spectrographs," in [*Optical Systems Design*], *Proc. SPIE* **8550** (2012).

[15] Stürmer, J., Stahl, O., Schwab, C., Seifert, W., Quirrenbach, A., Amado, P. J., Ribas, I., Reiners, A., and Caballero, J. A., "CARMENES in SPIE 2014. Building a fibre link for CARMENES," in [*Advances in Optical and Mechanical Technologies for Telescopes and Instrumentation*], *Proc. SPIE* **9151**, 915152 (July 2014).

[16] Avila, G., "FRD and scrambling properties of recent non-circular fibres," in [*Ground-based and Airborne Instrumentation for Astronomy IV*], *Proc. SPIE* **8446**, 84469L (Sept. 2012).